Journal of Power Sources 234 (2013) 16–22

Contents lists available at SciVerse ScienceDirect

Journal of Power Sources

journal homepage: www.elsevier.com/locate/jpowsour

Preparation of nanoporous TiO_2 films for DSSC application by a rapid atmospheric pressure plasma jet sintering process

Haoming Chang [a], Yao-Jhen Yang [b], Hsin-Chieh Li [b], Cheng-Che Hsu [b,1], I-Chun Cheng [c,d], Jian-Zhang Chen [a,*]

[a] Graduate Institute of Applied Mechanics, National Taiwan University, Taipei 10617, Taiwan
[b] Department of Chemical Engineering, National Taiwan University, Taipei 10617, Taiwan
[c] Graduate Institute of Photonics and Optoelectronics, Taipei 10617, Taiwan
[d] Department of Electrical Engineering, Taipei 10617, Taiwan

HIGHLIGHTS

- Atmospheric pressure plasma jet (APPJ) sintered nanoporous TiO_2 layers are studied.
- 60-s APPJ sintering can replace conventional 15 min, 510 °C calcination of TiO_2.
- The DSSCs with APPJ sintered TiO_2 photoanodes exhibit comparable cell efficiency.

GRAPHICAL ABSTRACT

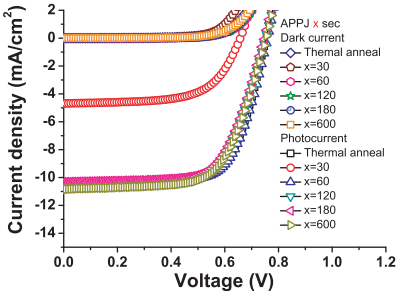

ARTICLE INFO

Article history:
Received 29 September 2012
Received in revised form
7 January 2013
Accepted 20 January 2013
Available online 1 February 2013

Keywords:
Atmospheric pressure plasma jet
Sintering
Titania
Nanoporous
Photoanode
Dye-sensitized solar cells

ABSTRACT

We investigate the nanoporous TiO_2 films sintered by atmospheric pressure plasma jets (APPJs) and their applications as photoanodes of dye-sensitized solar cells (DSSCs). A 30-s APPJ-sintered nanoporous TiO_2 layer exhibits an additional absorption band between 400 and 500 nm in wavelength, attributed to incomplete removal of the organic solvents in the pastes. For TiO_2 layers sintered by APPJs for 60 s and beyond, the absorption spectra are nearly identical to those of a conventional 15 min, 510 °C calcined sample. The XRD and XPS results indicate similar characteristics for APPJ-sintered and furnace-sintered TiO_2 films. A DSSC with a 30-s APPJ-sintered TiO_2 photoanode shows poor cell efficiency with an extremely large TiO_2/dye/electrolyte electron transport interfacial resistance and a short carrier lifetime. As the APPJ treatment time reaches 60 s and beyond, the power conversion efficiencies become comparable to that of a sample with a 510 °C conventionally calcined TiO_2 photoanode. Our experimental results verify that a 60-s APPJ sintering process is sufficient to replace a conventional 15 min, 510 °C furnace calcination process for TiO_2 photoanodes of DSSCs. The ultra-short sintering process is made possible by the synergistic effect of the temperature and the reactivity of the APPJ, which can lower the fabrication cost.

1. Introduction

Since the achievement of the major breakthrough in dye-sensitized solar cells (DSSCs) in 1991, this type of photovoltaic cell is becoming a rapidly emerging technology [1,2]. DSSC technology is environmentally friendly and potentially cost effective;

* Corresponding author. Graduate Institute of Applied Mechanics, National Taiwan University, No.1 Sec. 4 Roosevelt Rd., Taipei City 10617, Taiwan. Tel./fax: +886 2 3366 5694.
E-mail addresses: chsu@ntu.edu.tw (C.-C. Hsu), jchen@ntu.edu.tw (J.-Z. Chen).
[1] Department of Chemical Engineering, National Taiwan University, No.1 Sec. 4 Roosevelt Rd., Taipei City 10617, Taiwan. Tel.: +886 2 3366 3034; fax: +886 2 2362 3040.

0378-7753/$ – see front matter © 2013 Elsevier B.V. All rights reserved.
http://dx.doi.org/10.1016/j.jpowsour.2013.01.113

the cost of DSSCs can be further reduced if the price of high-performance dyes can be lowered. A 3-D network nanoporous photoanode is important in achieving high cell efficiency. Therefore, research efforts focusing on the design and fabrication of photoanodes have been emphasized [3–14]. Some techniques such as inverse opal photoanode structures [13,15–17], laser treatments [3,7–9], nanotube photoanode structures [4,11], microcavity embedded photoanodes [5,18,19], and over-layer coated photoanodes [6], have been extensively studied. In terms of photoanode processes, temperature and time are two key fabrication parameters. The processing temperature control is essential for the adjustment of the phases of the photoanodes. Furthermore, it is also critical for the fabrication of flexible DSSCs on plastic substrates owing to their low melting points [20–27]. Processing time is another critical issue in regard to industrial fabrications. The cost will be greatly lowered as the processing time is reduced.

Atmospheric pressure plasma technology is advantageous in versatile applications such as surface modification, thin film deposition, and nanoparticle fabrication [6,28–32]. Atmospheric pressure plasma jets (APPJs) consist of highly reactive plasmas, rendering rapid processing capability. In addition, it is a large-area compatible non-vacuum process, making this process more attractive in the fabrication of DSSCs. In this study, we take advantage of this feature to conduct rapid sintering of nanoporous TiO_2 photoanodes for DSSCs. The temperature of the substrate surface is controlled at around 500 °C during the APPJ sintering process. The results demonstrate that a merely 60-s APPJ treatment can fully convert screen-printed TiO_2 pastes into functional nanoporous TiO_2 photoanodes for DSSCs. In comparison, conventional furnace calcination processes have sintering times of at least 15 min excluding the ramping and cooling time control that prevents TiO_2 photoanodes from cracking.

2. Experimental details

A commercial TiO_2 paste (E-solar P300, Everlight Chemical Industrial Co.) was used in this study. The TiO_2 paste was screen-printed on the fluorine-doped tin oxide (FTO, sheet resistance 8 Ω cm, Pilkington Group Ltd.) glass with an area of 0.22 cm^2. The thickness of the deposited TiO_2 layer was approximately 10 μm. The printed TiO_2 was then sintered by APPJ in an N_2 atmosphere at a temperature of 500 °C for 30 s, 60 s, 120 s, 180 s, and 600 s. The detailed APPJ system is described in ref. [31], and the schematic APPJ apparatus is shown in Fig. 1(a). The APPJ system was operated with a 31 slm nitrogen gas flow, a 275 V applied voltage, and a 7/33 μs on/off duty cycle. The sample for APPJ-sintering process was located on the x–y stage moving toward the plasma jet with a velocity of 3 cm min^{-1}. The stage advancing time was around 2 min to prevent the film from cracking, and the film was sintered for designated durations under the plasma jet; the stage was retreated at the same velocity after the sintering process. The distance between the stage and the nozzle of the plasma jet was set as 2.7 cm, and the gap between the glass tube exit and the stage was 1 mm. A typical temperature evolution profile for a 60 s APPJ anneal is shown in Fig. 1(b). The temperature was measured by a K-type thermal couple in contact with the substrate as the APPJ is operated; the data are acquired and processed by a data acquisition device (USB-6221, National Instruments) and a computer. For comparison, the reference counterpart was sintered at 510 °C in air for 15 min using a tube furnace.

To fabricate DSSCs, the sintered TiO_2 nanoporous films were immersed in a mixed solution of acetonitrile (99.9%, J. T. Baker) and tertiary butyl alcohol (99.9%, J. T. Baker) containing 3×10^{-4} M of N719 dye (Solaronix) for 24 h. After the anchoring of dyes, the photoanodes were rinsed with ethanol and dried at room

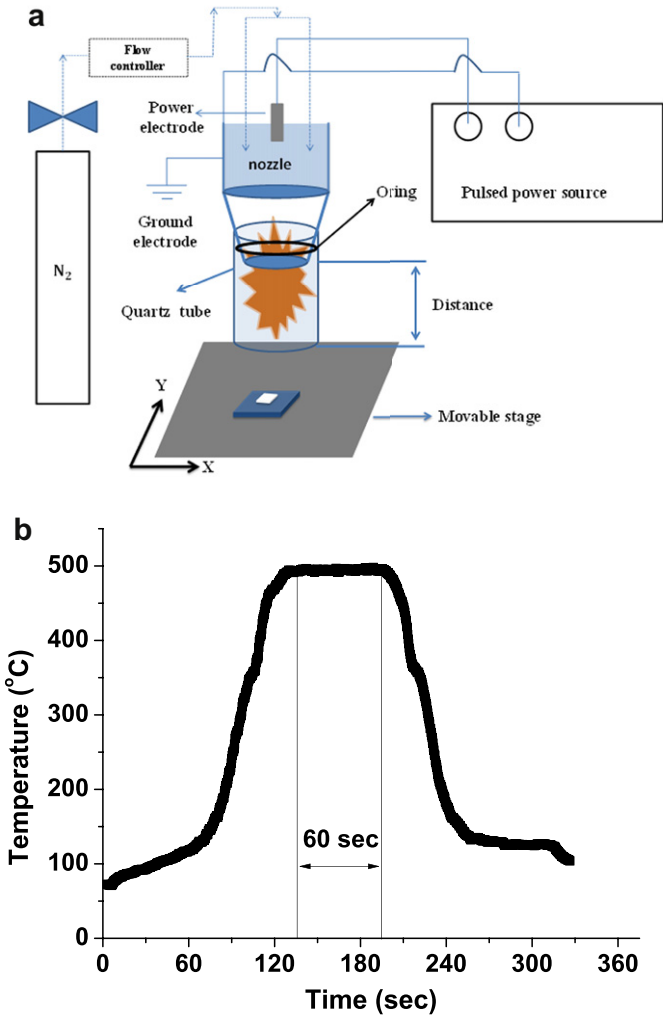

Fig. 1. (a) The schematic representation of the APPJ apparatus. (b) Substrate temperature evolution profile of APPJ sintering for 60 s.

temperature. The counter electrodes were fabricated by sputtering a 10 nm Pt layer onto an FTO glass substrate, which was then assembled with the dye-absorbed photoanode. Finally, liquid electrolyte (Eversolar EL 100, Everlight Chemical Industrial Co.), consisting of I_2, LiI, guanidinium thiocyanate (GuNCS) and acetonitrile, was injected into the assembled cells.

The TiO_2 films were examined by scanning electron microscopy (SEM, Nova NanoSEM 230, FEI) and X-ray diffraction (XRD, PANalytical X'Pert PRO). An ultraviolet–visible–near-infrared spectrophotometer (JASCO V-670) was used to determine the absorption spectra of nanoporous TiO_2 layers. The surface elemental composition was determined by XPS (VG ESCA Scientific Theta Probe). The C1s peak at binding energy of 285.0 eV was used to calibrate the shift of spectra.

For the power efficiency measurements of DSSCs, the cells were illuminated through the FTO glass substrates using a solar simulator (WACOM, WXS-155S-L2) with an AM1.5 filter. A Keithley 2400 electrometer was used to evaluate the I–V characteristics. Electrochemical impedance spectroscopy (EIS) analysis was performed using an electrochemical workstation (Zahner Zennium). The EIS spectra were obtained by applying sinusoidal perturbations of ±10 mV with frequencies ranged from 0.1 to 10^5 Hz under illumination.

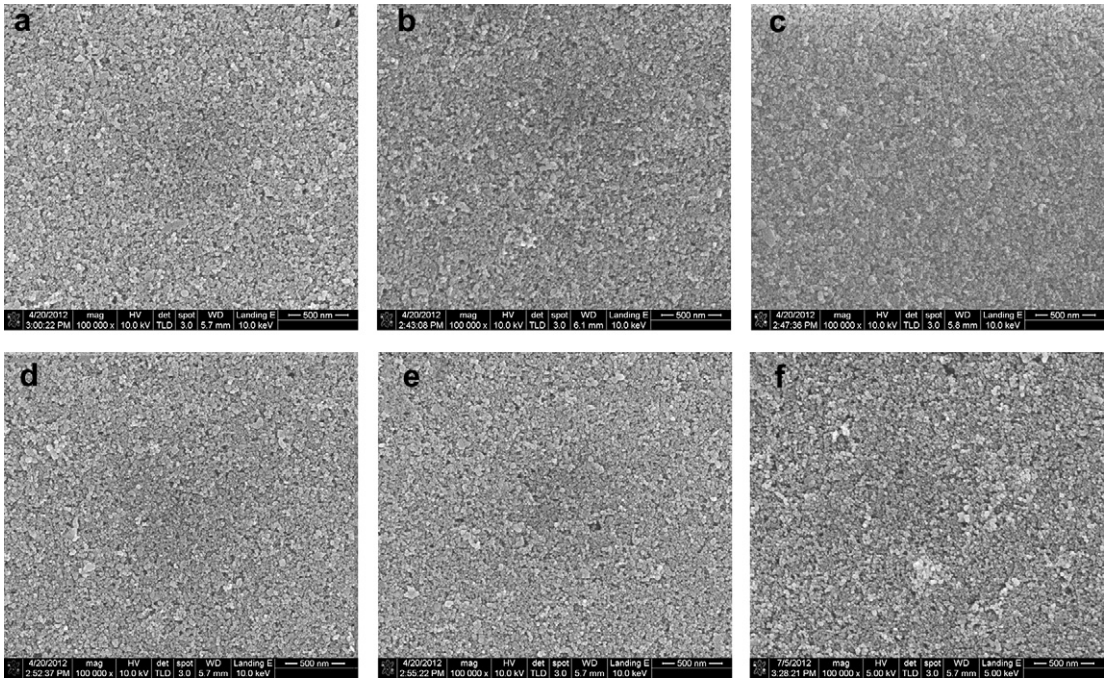

Fig. 2. SEM images of TiO_2 sintered by (a) 15 min, 510 °C thermal annealing, (b) APPJ 30 s treatment, (c) APPJ 60 s treatment, (d) APPJ 120 s treatment, (e) APPJ 180 s treatment and (f) APPJ 600 s treatment.

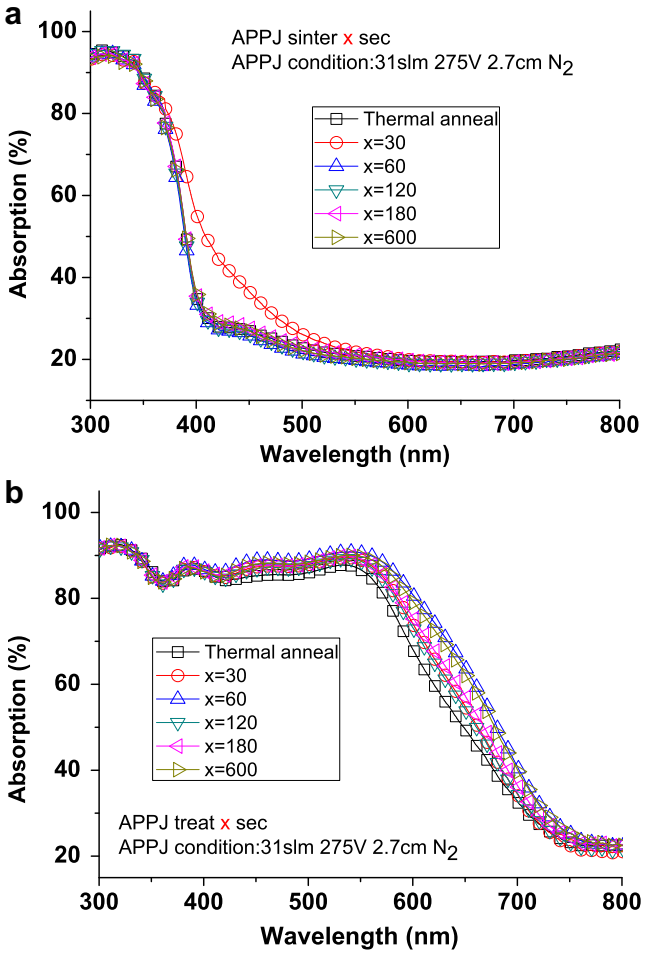

Fig. 3. UV–visible absorption spectra of (a) TiO_2 (b) dye-anchored TiO_2.

3. Results and discussion

Fig. 2 shows the SEM images of sintered nanoporous TiO_2 layers produced by the furnace-sintering and APPJ-sintering processes. No significant difference in morphology is observed among furnace-sintered and APPJ-sintered TiO_2 with various durations. Necking and agglomeration of TiO_2 nanoparticles are observed for all samples.

Fig. 3 shows the absorption spectra for pure and dye-anchored TiO_2. The absorption is calculated by $A = 1 - T - R$, where A is the absorption, T is the transmission, and R is the reflection. Both T and R are measured by using an integral sphere. For the absorption spectra of pure TiO_2 depicted in Fig. 3(a), the 30-s APPJ sintered TiO_2 exhibits an extra absorption tail from 400 to 500 nm. This indicates that 30 s APPJ sintering is insufficient to fully remove the organic solvent and to convert the screen-printed TiO_2 pastes. When the APPJ sintering time is around 60 s and beyond, the

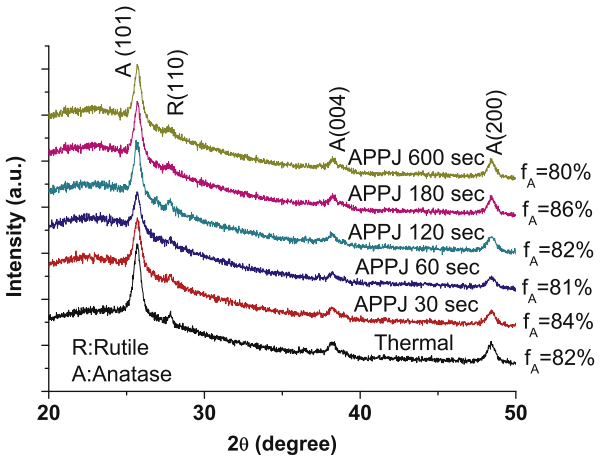

Fig. 4. XRD patterns of the TiO_2 layers sintered by furnace and APPJ.

Table 1
Grain size calculated from the diffraction peak of anatase (101).

	Grain size (nm)
Thermal anneal	17.6
APPJ 30 s	17.6
APPJ 60 s	18.7
APPJ 120 s	17.6
APPJ 180 s	17.3
APPJ 600 s	18.4

absorption spectra are almost identical to that of the furnace-sintered sample. Fig. 3(b) shows the absorption spectra of dye-anchored TiO_2. The absorption band is expanded by the dyes. APPJ-sintered TiO_2 layers with dyes have extra absorption between 550 and 750 nm compared with the furnace-sintered one, but the difference is small and within normal variation. Later we will show that this extra absorption for dye-anchored TiO_2 is insignificant in influencing DSSC performance.

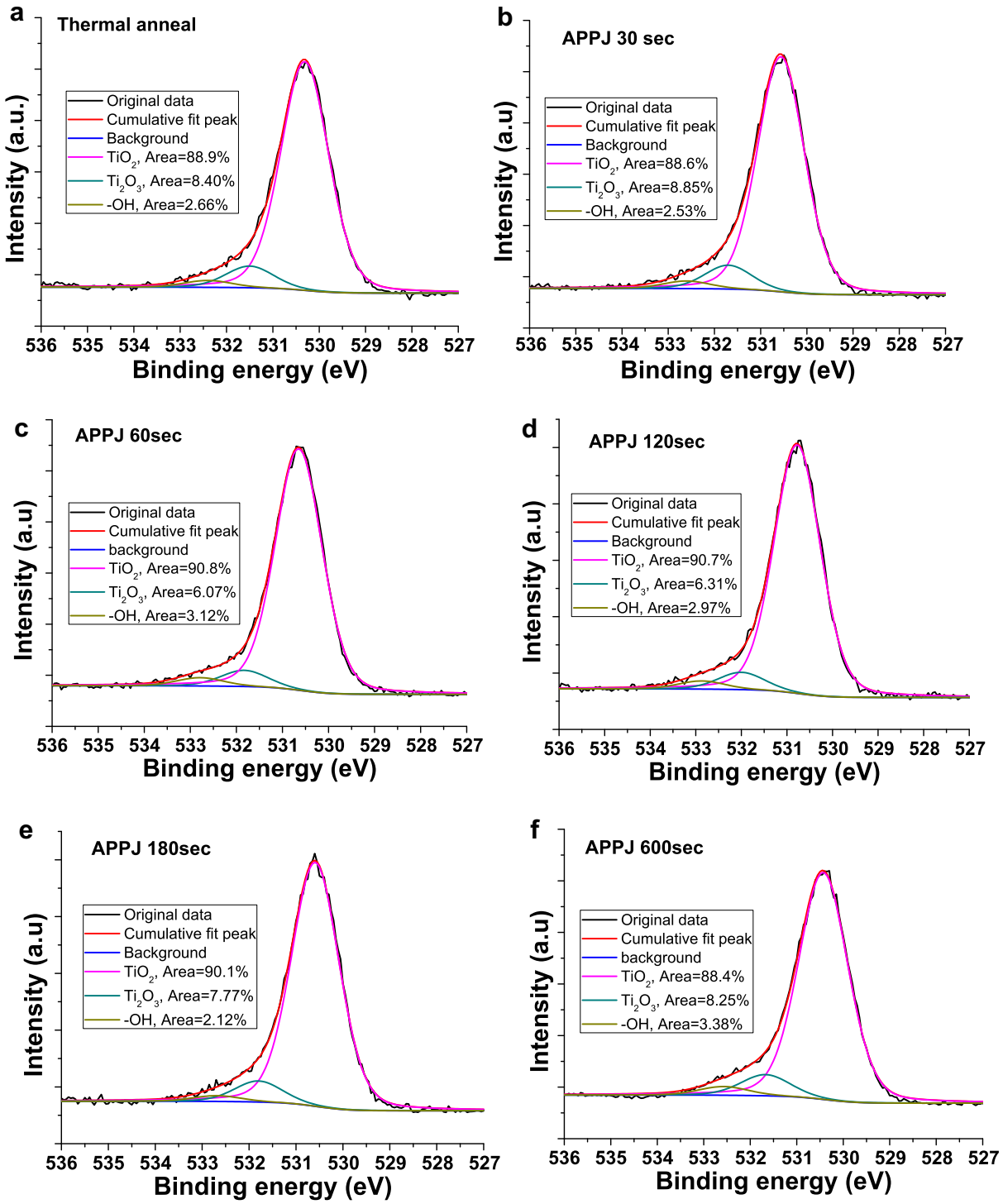

Fig. 5. High resolution O1s XPS spectra of the nanoporous TiO_2 layers sintered by (a) 15 min, 510 °C thermal annealing, (b) APPJ 30 s treatment, (c) APPJ 60 s treatment, (d) APPJ 120 s treatment, (e) APPJ 180 s treatment and (f) APPJ 600 s treatment.

Table 2
Surface state stoichiometry for TiO_2 layers.

	TiO_2 (%)	Ti_2O_3 (%)	−OH (%)
Thermal anneal	88.9	8.40	2.66
APPJ 30 s	88.6	8.85	2.53
APPJ 60 s	90.8	6.07	3.12
APPJ 120 s	90.7	6.31	2.97
APPJ 180 s	90.1	7.77	2.12
APPJ 600 s	88.4	8.25	3.38

Table 3
DSSC parameters extracted from Fig. 6.

	J_{SC} (mA cm)	V_{oc} (V) (v)	F.F	Efficiency (%)
Thermal anneal	10.4	0.750	0.685	5.37
APPJ 30 s	4.68	0.660	0.627	1.94
APPJ 60 s	10.5	0.759	0.688	5.51
APPJ 120 s	10.6	0.749	0.660	5.27
APPJ 180 s	10.3	0.747	0.665	5.13
APPJ 600 s	10.8	0.752	0.654	5.34

Fig. 4 shows the XRD patterns for furnace-calcined and APPJ-sintered TiO_2. The anatase content in the nanoporous TiO_2 can be estimated by Spurr and Myer's method [33] using the ratio of the two most intense peaks of anatase I_A (101) and rutile I_R (110). The anatase content f_A is described by the following equation

$$f_A = \frac{1}{1 + 1.26\, I_R/I_A} \quad (1)$$

The calculated values of f_A are listed by the XRD patterns shown in the same figure. No significant difference in f_A is observed among furnace-sintered and APPJ-treated TiO_2. The grain size d of the TiO_2 layer is estimated by Debye–Scherrer formula [34]

$$d = \frac{0.9\lambda}{\beta \cos\theta} \quad (2)$$

where λ is the Cu Kα X-ray wavelength (0.154 nm), β is the width at half maximum of the designated peak, and θ is the Bragg angle. The average grain sizes calculated from the diffraction peaks of anatase (101) are listed in Table 1. The grain sizes are comparable for furnace-sintered and APPJ-treated TiO_2.

It has been shown that the cell efficiency is strongly related to the oxygen vacancy Ti^{3+} state [35]. Therefore, the chemical surface states of the TiO_2 films are analyzed by XPS, as shown in Fig. 5. Three component peaks are resolved for the O1s peak. The main peak at ~530.5 eV indicates the lattice oxygen of TiO_2 with two shoulder peaks attributed to Ti_2O_3 (~531.5 eV) and −OH (~532.4 eV) respectively [35]. The surface state stoichiometry is estimated by relative peak areas as the percentage of the total area of the O1s peak. The analytical results are listed in Table 2. No significant difference in the surface state stoichiometry is observed among furnace-sintered and APPJ-sintered TiO_2 layers.

The above mentioned TiO_2 films are then used to assemble DSSCs. Fig. 6 shows representative IV characteristics of cells under dark and illumination environments. The cell parameters extracted from Fig. 6 are tabulated in Table 3. The photocurrent density, fill factor, and cell efficiency are comparable among DSSCs with furnace-sintered and APPJ-sintered TiO_2 photoanodes except for that with APPJ 30 s treatment. The DSSC that was given 30 s APPJ treatment, which showed extremely low efficiency, accompanied by low photocurrent density, open circuit voltage and fill factor. This is explained by its absorption spectra, which show incomplete conversion of TiO_2 pastes into nanoporous TiO_2 networks. This experiment was repeated several times, and the cell efficiency with an error bar is plotted in Fig. 7. The results solidly demonstrate that 60-s APPJ-sintering is sufficient to replace a 15-min furnace-calcination process for the preparation of nanoporous TiO_2 DSSC photoanodes. The much shorter time required for the APPJ-sintering process strongly suggests that the synergistic effect of the temperature and the reactivity of the APPJ [36,37] yields a rapid removal of organic solvent and a fast conversion of the screen-printed TiO_2 layers. N_2 plasmas are known for their high reactivity [38] because of the existing excited nitrogen molecules, as evidenced by the observation of N_2 1st positive ($B^3\Pi_g \rightarrow A^3\Sigma_u^+$) and N_2 2nd positive ($C^3\Pi_u \rightarrow B^3\Pi_g$) optical emission systems reported previously [37]. These excited state molecules possess energy over 6 eV above the ground state. Upon collision with the treated surface, the quenching of these molecules provides extra energy. The existence of excited nitrogen molecules together with the high jet temperature make the ultra-short processing time possible.

Fig. 8(a) presents the Nyquist plot of the EIS results of the DSSCs under light illumination of 100 $mWcm^{-2}$. The model equivalent circuit shown in Fig. 8(b) is described in detail in ref. [39]. Analysis of the system response contains the internal resistances and the electron transport kinetics in the DSSCs. Typically, three semicircles in the plot correspond to the interfaces of Pt/electrolyte and TiO_2/dye/electrolyte, as well as the Warburg diffusion process of I^-/I_3^-

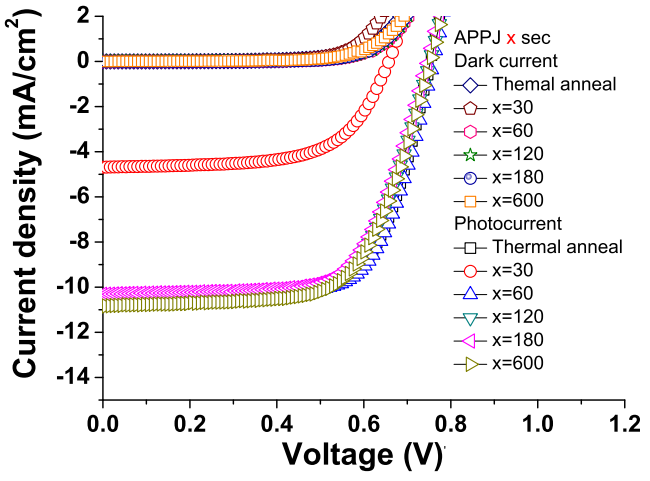

Fig. 6. Typical IV characteristics of DSSCs with furnace-sintered and APPJ-sintered TiO_2 photoanodes.

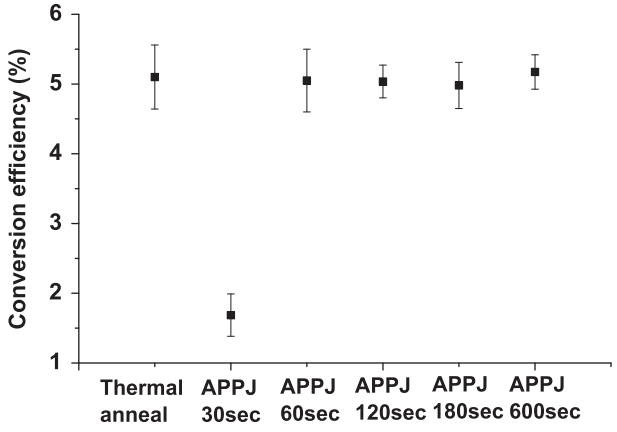

Fig. 7. Power conversion efficiency of DSSCs measured under AM1.5, 100 mW cm^{-2} conditions.

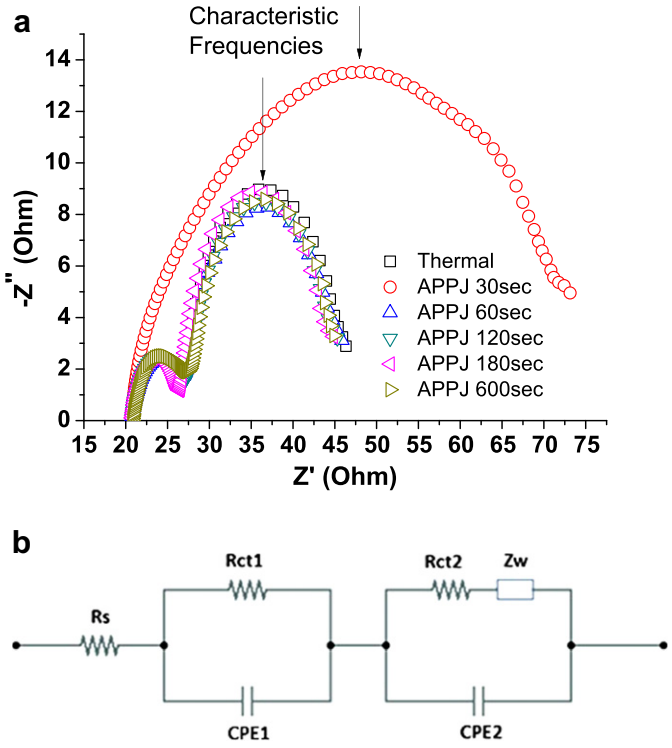

Fig. 8. (a) Nyquist plot of DSSCs with photoanodes sintered by furnace and APPJ under illumination. (b) The model equivalent circuit diagram.

Table 4
Impedances R_{ct2} of TiO_2/dye/electrolyte interface and electron lifetimes extracted from Fig. 8

	R_{ct2} (Ω)	Characteristic frequency (Hz)	Electron lifetime (ms)
Thermal anneal	22.7	14.2	11.2
APPJ 30 s	64.7	144	1.1
APPJ 60 s	23.9	9.99	15.9
APPJ 120 s	22.1	9.99	15.9
APPJ 180 s	21.9	12.0	13.3
APPJ 600 s	21.2	9.99	15.9

[40]. The first semicircle in the high frequency region corresponds to the impedance of the Pt/electrolyte interface, which has the smallest resistance in the DSSC. The middle semicircle represents the TiO_2/dye/electrolyte interface, with the circle diameter as the value of impedance R_{ct2}. The apex of the semicircle corresponds to a characteristic frequency, which can be related to the inverse of the electron lifetime (τ_e) in the TiO_2 films. The calculated R_{ct2} and τ_e for various experimental conditions are listed in Table 4. An extremely large charge transfer resistance R_{ct2} is observed for the DSSC with 30-s APPJ-sintered TiO_2 photoanode, which may be attributed to the incomplete removal of the organic components from the pastes. The other cases studied show similar EIS spectra and R_{ct2} values. The electron lifetime for the 30-s APPJ-sintered case is also much shorter than the others. The lifetimes for DSSCs with APPJ treated photoanodes are slightly longer than that in the thermally-annealed case.

4. Conclusion

The screen-printed TiO_2 films sintered by APPJs were investigated and applied to DSSCs. A 30-s APPJ-sintered TiO_2 layer showed an extra absorption tail between 400 and 500 nm in wavelength, owing to the incomplete removal of the organic solvents in the pastes. For the cases with longer APPJ sintering durations, the absorption spectra were almost identical to that of a conventional 510 °C calcined case. The XRD and XPS results indicated similar phase structures and oxygen vacancy states for APPJ-sintered and furnace-sintered TiO_2 films. DSSCs with TiO_2 photoanodes prepared by 30 s APPJ-sintering showed much lower power conversion efficiency than those with furnace-calcined TiO_2. However, the assembled DSSCs exhibited comparable efficiencies when the TiO_2 layer was treated for 60 s or more by APPJ. The EIS results indicated that DSSCs with only 30 s APPJ-sintered TiO_2 photoanodes showed an extremely large TiO_2/dye/electrolyte electron transport interfacial resistance and a short carrier lifetime, owing to the incomplete removal of the organics in the pastes. In conclusion, our experimental results showed that a 60-s APPJ sintering process for TiO_2 was sufficient to replace a conventional 15 min 510 °C furnace calcination. The ultra-short APPJ sintering process time was made possible by the synergistic effect of the temperature and the reactivity of the plasma jet. The fabrication cost of DSSCs can be further reduced with the shorter TiO_2 preparation time.

Acknowledgments

The authors gratefully acknowledge the funding supports from the National Science Council of Taiwan under the grant nos. NSC 101-2221-E-002-096 (JZC); NSC 100-2221-E-002-151-MY3 and NSC 100-3113-E-002-012 (ICC).

References

[1] B. O'Regan, M. Gratzel, Nature 353 (1991) 737–740.
[2] M. Grätzel, Progress in Photovoltaics: Research and Applications 14 (2006) 429–442.
[3] M.-Y. Pu, J.Z. Chen, Materials Letters 66 (2012) 162–164.
[4] A.B.F. Martinson, J.W. Elam, J.T. Hupp, M.J. Pellin, Nano Letters 7 (2007) 2183–2187.
[5] D.-W. Liu, I.C. Cheng, J.Z. Chen, H.-W. Chen, K.-C. Ho, C.-C. Chiang, Optics Express 20 (2012) A168–A176.
[6] J. Tak Kim, S. Ho Kim, Solar Energy Materials and Solar Cells 95 (2011) 336–339.
[7] H. Kim, G.P. Kushto, C.B. Arnold, Z.H. Kafafi, A. Pique, Applied Physics Letters 85 (2004) 464–466.
[8] H. Kim, R.C.Y. Auyeung, M. Ollinger, G.P. Kushto, Z.H. Kafafi, A. Piqué, Applied Physics A: Materials Science & Processing 83 (2006) 73–76.
[9] H. Pan, S.H. Ko, N. Misra, C.P. Grigoropoulos, Applied Physics Letters 94 (2009) 071113–071117.
[10] G. Mincuzzi, L. Vesce, A. Reale, A. Di Carlo, T.M. Brown, Applied Physics Letters 95 (2009) 103312–103313.
[11] R.B. Tao, T. Tomita, R.A. Wong, K. Waki, Journal of Power Sources 214 (2012) 159–165.
[12] W.K. Tu, C.J. Lin, A. Chatterjee, G.H. Shiau, S.H. Chien, Journal of Power Sources 203 (2012) 297–301.
[13] J.G. Yu, J.J. Fan, B. Cheng, Journal of Power Sources 196 (2011) 7891–7898.
[14] C.P. Lee, L.Y. Lin, K.W. Tsai, R. Vittal, K.C. Ho, Journal of Power Sources 196 (2011) 1632–1638.
[15] P.R. Somani, C. Dionigi, M. Murgia, D. Palles, P. Nozar, G. Ruani, Solar Energy Materials and Solar Cells 87 (2005) 513–519.
[16] C.L. Huisman, J. Schoonman, A. Goossens, Solar Energy Materials and Solar Cells 85 (2005) 115–124.
[17] S. Dadgostar, F. Tajabadi, N. Taghavinia, ACS Applied Materials & Interfaces 4 (2012) 2964–2968.
[18] Y.C. Hsu, T.C.C. Wu, I.C. Cheng, J.Z. Chen, M.R. Yang, Japanese Journal of Applied Physics 50 (2011).
[19] J.Z. Chen, Y.C. Hsu, I.C. Cheng, Electrochemical and Solid-State Letters 14 (2011) B6–B8.
[20] M. Berginc, U. Opara Krašovec, M. Hočevar, M. Topi&ccaron, Thin Solid Films 516 (2008) 7155–7159.
[21] T. Miyasaka, Y. Kijitori, T.N. Murakami, M. Kimura, S. Uegusa, Chemistry Letters 31 (2002) 1250–1251.
[22] P. Balraju, P. Suresh, M. Kumar, M.S. Roy, G.D. Sharma, Journal of Photochemistry and Photobiology A: Chemistry 206 (2009) 53–63.
[23] F. Pichot, J.R. Pitts, B.A. Gregg, Langmuir 16 (2000) 5626–5630.
[24] C. Longo, A.F. Nogueira, M.-A. De Paoli, H. Cachet, The Journal of Physical Chemistry B 106 (2002) 5925–5930.
[25] D. Zhang, T. Yoshida, H. Minoura, Advanced Materials 15 (2003) 814–817.

[26] K.M. Lee, W.H. Chiu, M.D. Lu, W.F. Hsieh, Journal of Power Sources 196 (2011) 8897–8903.
[27] H.W. Chen, C.Y. Lin, Y.H. Lai, J.G. Chen, C.C. Wang, C.W. Hu, C.Y. Hsu, R. Vittal, K.C. Ho, Journal of Power Sources 196 (2011) 4859–4864.
[28] R. Foest, E. Kindel, A. Ohl, M. Stieber, K.D. Weltmann, Plasma Physics Controlled Fusion 47 (2005) B525–B536.
[29] S.E. Babayan, J.Y. Jeong, A. Schutze, V.J. Tu, M. Moravej, G.S. Selwyn, R.F. Hicks, Plasma Sources Science and Technology 10 (2001) 573–578.
[30] Y.C. Hong, H.S. Uhm, Applied Physics Letters 89 (2006) 221504.
[31] Y.-W. Hsu, H.-C. Li, Y.-J. Yang, C.-C. Hsu, Thin Solid Films 519 (2011) 3095–3099.
[32] A. Schutze, J.Y. Jeong, S.E. Babayan, P. Jaeyoung, G.S. Selwyn, R.F. Hicks, IEEE Transactions on Plasma Science 26 (1998) 1685–1694.
[33] R.A. Spurr, Analytical Chemistry 29 (1957) 760–762.
[34] A.L. Patterson, Physical Review 56 (1939) 978–982.
[35] Y. Yu, K. Wu, D. Wang, Applied Physics Letters 99 (2011) 192103–192104.
[36] Y. Lin, Y.J. Yang, C.C. Hsu, Thin Solid Films 519 (2011) 3043–3049.
[37] Y.W. Hsu, Y.J. Yang, C.Y. Wu, C.C. Hsu, Plasma Chemistry and Plasma Processing 30 (2010) 363–372.
[38] A.N. Wright, C.A. Wrinkler, Active Nitrogen, Academic Press Inc., New York, 1968.
[39] K.-M. Lee, V. Suryanarayanan, K.-C. Ho, Solar Energy Materials and Solar Cells 91 (2007) 1416–1420.
[40] C.-P. Hsu, K.-M. Lee, J.T.-W. Huang, C.-Y. Lin, C.-H. Lee, L.-P. Wang, S.-Y. Tsai, K.-C. Ho, Electrochimica Acta 53 (2008) 7514–7522.